J Mater Sci (2011) 46:3066–3072
DOI 10.1007/s10853-010-5185-x

Three-primary-color upconversion luminescence in rare earth-doped β-$NaLuF_4$ microtubes

Congbing Tan · Yunxin Liu · Wenbin Li

Received: 12 October 2010 / Accepted: 9 December 2010 / Published online: 21 December 2010

Abstract Lanthanide ions-doped $NaLuF_4$ hexagonal-prismatic microtubes have been successfully synthesized via a facile hydrothermal approach for the first time. The as-grown microtubes are determined to be pure hexagonal (β-) $NaLuF_4$ phase with an outermost diameter of about 3 μm and a length of approximately 40 μm. The $Yb^{3+}/Er^{3+}(Tm^{3+})$-codoped $NaLuF_4$ microtubes emit bright three-primary-color (red, green, and blue) light under 980 nm laser diode excitation undergoing an upconversion. Mechanisms for the excitation and emission were analyzed based on the emission spectra, the plot of luminescence intensity to pump power and a simplified energy level diagram.

Introduction

Lanthanide-doped fluorides with general formula like $NaReF_4$ [rare earth (Re)], especially $NaYF_4$, have received increasing attention for their potential applications in fields such as colorful displaying [1], solid state lasers [2], three dimensional imaging [3, 4], and bio-sensors [5, 6]. Among the $NaReF_4$, the $NaLuF_4$ has been attracted considerable interests due to its unique optical properties: first, Lu^{3+} ion can sensitize the codoped emitters to broaden the emission spectra or enhance the emission intensity [7]; second, Lu^{3+} ion doping will take a volume compensation to improve the optical performance [8]; third, the mechanical properties of optical materials can be readily enhanced by doping Lu^{3+} ion to adjust the retardation of grain boundary diffusion which will result in the high modulus of anti-creep deformation to ensure the promising optical performance at high temperatures [9]. Furthermore, it was found that Lu^{3+} ion doping can affect the emitter's electronic population lifetime so that the luminescence properties, such as brightness and long afterglow performance, was remarkably tuned [10]. In a word, Lu^{3+} ion has a lot of special physical, chemical, and optical properties. Therefore, the Lu^{3+}-doped materials or its compounds have distinct performances in the optical fields with other systems. Recently, the hexagonal (β-) $NaLuF_4$, which has the same space group ($P6_3/m$) and crystalline planes as β-$NaYF_4$ [11], is confirmed to be a type of idea host lattice for visible up- and down-conversion fluorescence [12, 13]. In this study, we show the three-primary-color luminescence $NaLuF_4$ by doping with Yb/Tm or Yb/Er or their couples, in which some unexpected optical properties were observed with respect to the commonly reported results.

Compared with two-dimensional (2D) nano- and microstructures, the 1D structure with hollow interiors, such as nanotubes, microtubes, and hollow spheres, has been considered to be beneficial to save raw materials and may lead to novel and excellent optical properties [14, 15]. Recently, considerable effort has been devoted to the exploration of various convenient and efficient approaches for synthesizing $NaReF_4$ micro- and nano-tubes [11, 12, 16–19]. Zhang et al. [20] recently reported the preparation of $NaYF_4$ nanotubes by in situ ion exchange. Liang et al. [21] reported the hydrothermal synthesis of the $NaHoF_4$ microtubes and $NaSmF_4$ nanotubes. Among the reported synthesis techniques, hydrothermal method as a low-lost and high-yield approach has been proven to be a facile and

C. Tan (✉) · Y. Liu · W. Li
School of Physics, Hunan University of Science and Technology, Xiangtan, Hunan 411201, China
e-mail: cbtan@hnust.edu.cn

Y. Liu
Institute of Modern Physics, Xiangtan University, Xiangtan, Hunan 411201, China

general process for the synthesis of nano- and micro-sized fluorides with special morphologies and architectures [16, 22].

Although the physical, chemical, and optical properties of Lu^{3+} ion or its compounds have been investigated in a wide range, no report concerning the direct facile synthesis and three-primary-color upconversion of well-defined and uniform $NaLuF_4$ microtubes was presented to push the real application of the Re-doped $NaLuF_4$ forward. Accordingly, we report for the first time the preparation of β-$NaLuF_4$ microtubes via a facile hydrothermal method. The upconversion emission and their possible mechanisms for the Yb^{3+}, Tm^{3+}, Er^{3+}-doped β-$NaLuF_4$ microtubes were investigated in details.

Experimental

Sample preparation

The analytical grade reagents were used as the raw materials without further purification. $Ln(NO_3)_3$(Ln = Lu, Yb, Er, Tm) aqueous solution were obtained by dissolving Ln_2O_3 (Ln = Lu, Yb, Er, Tm: 99.99%) in a minimum amount of nitric acid (1:1.2) and evaporated to dryness, then dissolved in distilled water to form Re nitrate solutions.

In a typical procedure for the preparation of $NaLuF_4$:20% Yb^{3+}/2% Er^{3+} microtubes, 0.936 mL of $Lu(NO_3)_3$ (0.5 M), 0.6 mL of $Yb(NO_3)_3$ (0.2 M), and 0.12 mL of $Er(NO_3)_3$ (0.1 M) were added into 30 mL aqueous solution containing 1.2 mmol tri-sodium citrate. After stirring for 10 min, 9 mL NaF aqueous solution (0.8 M) was introduced into the above solution. The pH value was adjusted at 1–2 through dropping dilute HNO_3 or NaOH solution. After another agitation for 10 min, the resulting precursor solution was transferred to a stainless steel autoclave with Teflon linear of 40 mL capacity and heated at 200 °C for 4 h in a digital type temperature-controlled oven. After the autoclave was cooled down to room temperature naturally, the resulting product was separated centrifugally and washed with distilled water and then with absolute ethanol three times. Subsequently, the product was dried at 60 °C for 12 h to obtain $NaLuF_4$:20% Yb^{3+}/2% Er^{3+} microtubes. The preparation of the samples with other dopant is similar to the above procedure.

Characterization

The phase structure and purity of the as-prepared samples were characterized using X-ray diffraction (XRD) on a Bruker/AXS D8-ADVANCE X-ray diffractometer using a copper target ($\lambda = 0.15405$ nm) for 2θ ranging from 15° to 70°. The particles sizes and morphologies of the samples were determined using scanning electron microscopy (SEM) on a JOEL JSM-6380LV working at 30 kV. Upconversion fluorescence spectra of the samples under excitation of 980 nm laser diode (LD) were recorded with a Jobin-Yvin U1000 spectrometer equipped with a Photocool PC104CE photomultiplier tube. The power of LD was determined by a ThorLab 121 power meter. All the tests were performed at the ambient temperature.

Results and discussion

Phase identification and morphology

The XRD profiles in Fig. 1 show that the diffraction peak from 15° to 70° agree well with those of the hexagonal (β-) $NaLuF_4$ with calculated lattice constants of $a = 5.939$ Å and $c = 3.450$ Å, which is very close to the standard data reported in literature (JCPDS No. 27-0726, $a = 5.901$ Å and $c = 3.453$ Å). No additional peaks are observed, which indicates the high purity of the final product. It is also worthwhile to note that the diffraction peaks of the sample are very sharp and strong, suggesting that the products with high crystallinity can be prepared using this simple method. This is important for the luminescence materials, because higher crystallinity generally means fewer defect traps and higher emission efficiency [12].

The low-magnification SEM image (Fig. 2a) reveals that the products have tubular morphology with sharp ends. From local magnified SEM images (Fig. 2b, c), we can see that the sample consists of mean 3 × 40 μm (diameter × length) size hollow hexagonal-prismatic tubes. To the best of our knowledge, this structural β-$NaLuF_4$ is the first time successfully synthesized. The investigation of the growth

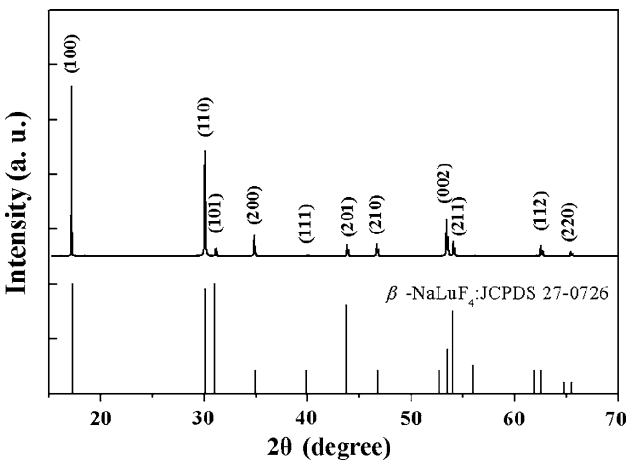

Fig. 1 XRD patterns of the as-obtained $NaLuF_4$ sample and the standard data of β-$NaLuF_4$ (JCPDS 27-0726) as a reference

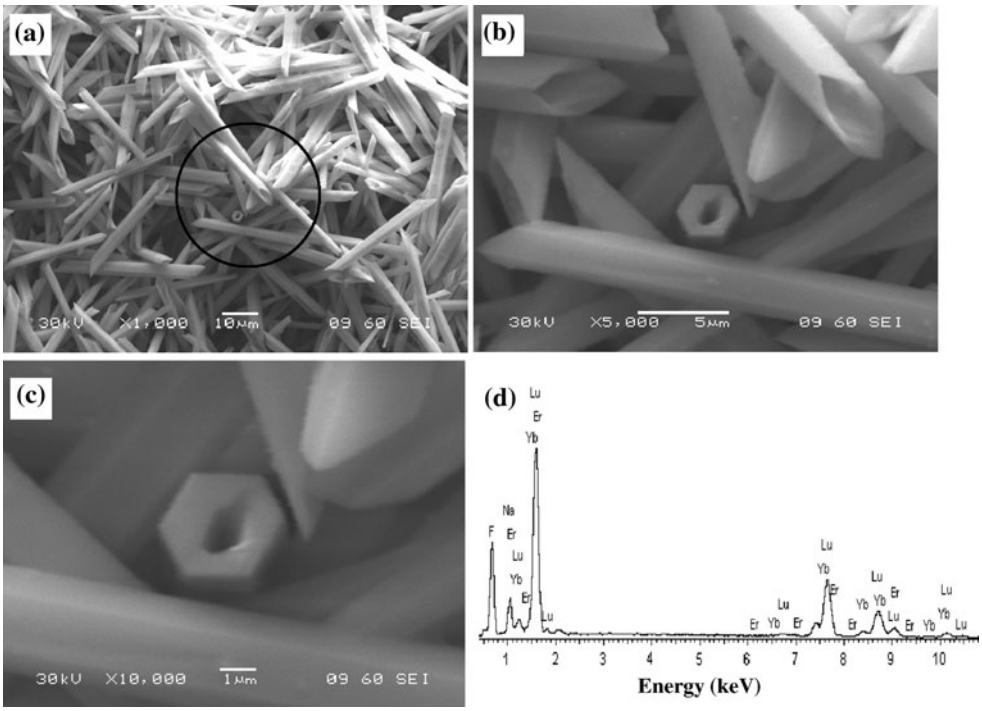

Fig. 2 **a** SEM image, **b** local magnified SEM image, **c** high-magnified SEM image, and **d** EDS spectrum of the as-prepared β-$NaLuF_4$ product

mechanism is in progress. In general, hollow structural tube can save the expensive raw materials as well as improve luminescence efficiency [20, 23]. The stronger interaction between the under coordinated atoms also tune the luminescence energy by varying the fraction of such atoms in the specimen [24, 25]. Figure 2d shows the EDS pattern for the β-$NaLuF_4$ microtubes, which exhibits the presence of Na, Lu, F, Yb, and Er, indicating that the Yb^{3+} and Er^{3+} ions have been effectively incorporated into the host lattice of the β-$NaLuF_4$, which is in accord with the above XRD results.

Upconversion luminescence

It is well known that the lanthanide (Yb, Tm, and Er) were generally used to dope fluorides to obtain blue (from Tm^{3+}), green (Er^{3+}), and red (Er^{3+}) upconversion luminescence, which are the three-primary-color [17, 26–28]. Lu^{3+} is also a type of lanthanide ion whose compounds are confirmed to be an efficient host material for upconversion luminescence [12, 13]. The reported study showed that $NaLuF_4$ plates and wires could be produced in the condition of properly adjusted chemical and physical reaction systems. However, $NaLuF_4$ tube structure has not been found in so far from the open literature. Here, we present the synthesis of uniform β-$NaLuF_4$ microtubes and their upconversion luminescence properties upon the doping of the Yb^{3+}/Tm^{3+}, Er^{3+}, Yb^{3+}/Er^{3+} couples, which demonstrates the benefit of employing the $NaLuF_4$ as a host material.

β-$NaLuF_4$ doped with Yb^{3+}/Tm^{3+}: Tm^{3+} ion is an efficient emitter for the energy upconverting blue luminescence, which is ascribed to its dominant inter-4*f* transition of $^1G_4 \rightarrow {}^3H_6$. Yb^{3+} ion is codoped to sensitize Tm^{3+} ion to enhance the luminescence efficiency of Tm^{3+} ion. The upconversion emission spectra for the β-$NaLuF_4$:20% Yb^{3+}/*x*% Tm^{3+} ($x = 0.2, 0.5, 0.8, 1.0, 1.5$, and 3.0) were measured under 980 nm infrared LD excitation with power of 120 mW as shown in Fig. 3. In the range of visible light spectrum, three emission bands, centered at 450, 478, and 649 nm dominate the emission spectra of Tm^{3+} in the Yb^{3+}/Tm^{3+} co-doped $NaLuF_4$ microtubes. The strong blue emission bands can be correspondingly assigned to the $^1D_2 \rightarrow {}^3F_4$ and $^1G_4 \rightarrow {}^3H_6$ transitions of Tm^{3+}, while the relatively weaker red emission is attributed to the $^1G_4 \rightarrow {}^3F_4$ transition. From Fig. 3, it is observed that the luminescence intensity of all emission bands of Tm^{3+} ion strongly depends on the concentration of the doped-Tm^{3+} ion. For red emission band centered at 649 nm, the strongest emission intensity was generated with the doping of 0.5 mol% Tm^{3+} when the concentration of Tm^{3+} ion varied between 0.2 and 3 mol%. Interestingly, the condition is changed for 478 and 450 nm blue emission bands, which corresponded to 0.8 and 0.2 mol% Tm^{3+} ion, respectively. The intensity ratio of 478 nm blue band to 649 nm red band was found to take a variation of increasing first with increasing the Tm^{3+} content and subsequently decreasing with further increasing the Tm^{3+} content. For this variation of intensity ratio, it is suggested that a competition readily occurred between $^1G_4 \rightarrow {}^3H_6$ and $^1G_4 \rightarrow {}^3F_4$ transitions which would

determine the variation of corresponding intensity ratio. It is well known that the $^1G_4$ level of Tm^{3+} can depopulate $^3H_6$ state to emit ~480 nm blue light and simultaneously the $^3F_4$ state to emit ~650 nm red light. With increasing Tm^{3+} content, the dipole-quadruple $^1G_4 \rightarrow {}^3H_6$ transition is predominantly promoted due to the enhanced energy transfer between Tm^{3+} pairs, while the dipole–dipole $^1G_4 \rightarrow {}^3H_4$ transition is less affected by the improved energy transfer between Tm^{3+} pairs induced by increasing concentration of Tm^{3+}. As a result, it was observed that the intensity ratio of 478 nm blue light to 650 nm red light increases with Tm^{3+} content increasing from 0.2 to 0.8 mol%. However, as the concentration of Tm^{3+} exceeds 0.8 mol%, the concentration quenching occurred considerably, which leads to the decrease of the luminescence intensity of highly concentration-dependent $^1G_4 \rightarrow {}^3H_6$ transition. Thus, it was observed that the intensity ratio of the 478 nm blue light to the 650 nm red light decrease with increasing Tm^{3+} content higher than 0.8 mol%. The total integral intensity was measured for each synthesized samples with different doping levels of Tm^{3+} ions as shown in the inset of Fig. 3. It is clear that the emission intensity goes up remarkably with the Tm^{3+} concentration up to 0.8 mol%. However, as the content further increasing to 1.0 mol%, the integral luminescence intensity dramatically decreases, which results from the quenching of fluorescence [29]. The variation of the integral luminescence intensity has also confirmed the presence of the threshold of 0.8 mol%, higher than which the remarkable concentration quenching phenomenon will occur. This is in good agreement with the above analysis on the variation of intensity ratio of $^1G_4 \rightarrow {}^3H_6$ to $^1G_4 \rightarrow {}^3F_4$ transition. When $NaLuF_4$:20% Yb^{3+}/0.8% Tm^{3+} microtubes was excited under 980 nm LD with a 120 mW power, the digital photograph has also been taken with 0.1 s exposure time as shown in the middle inset of Fig. 3, which demonstrates the blue dominant emission with high emission efficiency of $NaLuF_4$:20% Yb^{3+}/0.8% Tm^{3+} microtubes.

β-$NaLuF_4$ doped with Yb^{3+}/Er^{3+}: Different from Tm^{3+}, Er^{3+} can emit intense red and green lights under the infrared light which can produce three primary colors by combining with the blue emission of Tm^{3+}. Under a 980 nm LD excitation, the $NaLuF_4$:2% Er^{3+} emits three predominant bands arising from the 4*f* inter shell electronic transitions of Er^{3+} (Fig. 4a). Two green emission bands, centered at 520 and 540 nm, were assigned to the $^2H_{11/2} \rightarrow {}^4I_{15/2}$ and $^4S_{3/2} \rightarrow {}^4I_{15/2}$ transitions, respectively, while the red emission, centered at 658 nm, was attributed to the $^4F_{9/2} \rightarrow {}^4I_{15/2}$ transition of Er^{3+}. Comparing the emission spectra of $NaLuF_4$:20% Yb^{3+}/2% Er^{3+} with that of the $NaLuF_4$:2% Er^{3+} (Fig. 4), it is clear that the location of the red and the green bands have no evident changes. However, it was worth noting that the integral luminescence intensity of the Yb/Er-codoped sample was enhanced to be five times of that of singular Er^{3+} doped one. Furthermore, it is observed form Fig. 4 that the 410 nm emission peak arises in the Yb/Er-codoped $NaLuF_4$ originating form the transition o f $^2H_{9/2} \rightarrow {}^4I_{15/2}$ [30–33]. In general, the 410 nm emission could not be observed due to the low efficiency of three- or four-photon upconversion and strong scattering of host lattices. The observation of 410 nm emission gives a direct evidence for the high efficiency of $NaLuF_4$ host. For the difference between the Yb/Er-codoped and the Er^{3+} single-doped $NaLuF_4$, it can be elucidated as follows based on the energy transfer theory. The Er^{3+} exhibits usually low absorption cross section under a 980 nm LD excitation, leading to low upconversion efficiency. However, the $^2F_{7/2} \rightarrow {}^4F_{5/2}$ transition of Yb^{3+} ion

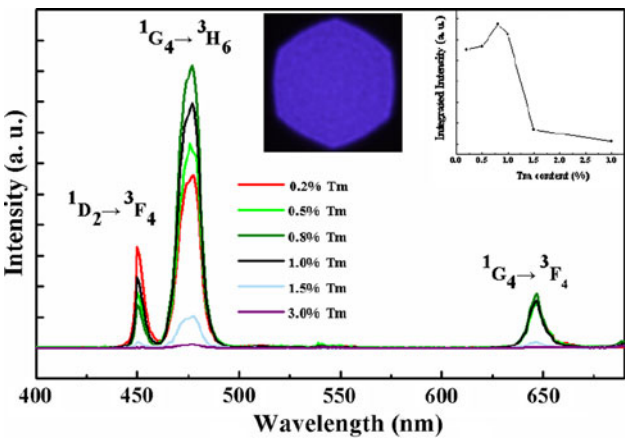

Fig. 3 Upconversion spectra of $NaLuF_4$:20% Yb^{3+}/*x*% Tm^{3+} ($x = 0.2$, 0.5, 0.8, 1.0, 1.5, and 3.0) microtubes under 980 nm LD excitation. *Insets* show the change of emission integral intensity with different Tm^{3+} concentration and the digital photograph of $NaLuF_4$:20% Yb^{3+}/0.8% Tm^{3+} microtubes

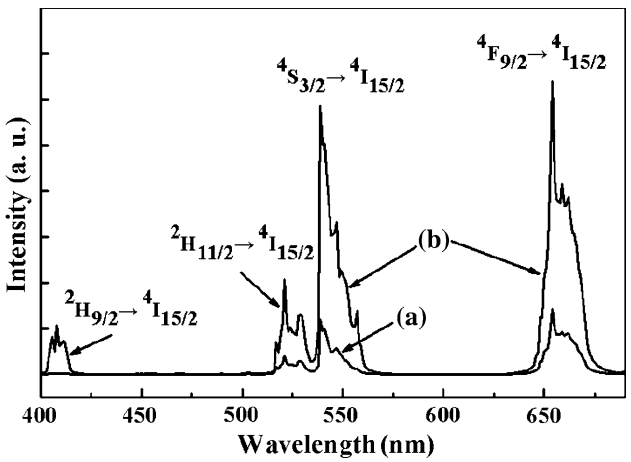

Fig. 4 Upconversion spectra of the $NaLuF_4$:2% Er^{3+} (*a*) and $NaLuF_4$:20% Yb^{3+}/2% Er^{3+} (*b*) samples under 980 nm LD excitation

has not only a large absorption cross section but also is well resonant with the 4*f* inter-shell transitions of the Er^{3+} ions [29], such as $^4I_{15/2} \rightarrow {}^4I_{11/2}$ and $^4I_{11/2} \rightarrow {}^4F_{7/2}$ which facilitates energy transfer from Yb^{3+} to Er^{3+} ions and results in the argument of the luminescence efficiency and the presence of the violet $^2H_{9/2} \rightarrow {}^4I_{15/2}$ emission. In fact, Yb^{3+} is commonly used as a sensitizer in the upconversion systems, which influences both the luminescence intensity and the intensity ratio of the red to the green emission. In order to investigate further the role of Yb^{3+} played in the upconversion systems, the $NaLuF_4$:Yb^{3+}/Er^{3+} with various doping levels of Yb^{3+} was synthesized, of which the emission spectra is shown in Fig. 5. It can be seen that the red to the green intensity was considerably improved with increasing the Yb^{3+} concentration from 0 to 100 mol%. Actually, the emission mechanisms resulting in the increase of the red to green intensity ratio have been discussed intensively suggesting in most cases that the concentration quenching will occur for the high doping level of Yb^{3+}. However, the concentration quenching was not obviously observed even in the $NaYbF_4$:Er^{3+}, demonstrating the distinct upconversion luminescence mechanism, e.g., deleterious cross-relaxation in the excessively high concentration of Yb^{3+} [29]. Combing with the crystal field environment factor, it can be elucidated that the Yb^{3+} plays multi-roles of both sensitizer and host material, which not only improves the luminescence efficiency of the Er^{3+} ion, but also supplies Er^{3+} ion with an efficient crystal field for energy transfer and luminescence [34]. The digital photographs in the inset of Fig. 5 show green, yellow, and red luminescence of $NaLuF_4$:20% Yb^{3+}/2% Er^{3+}, $NaLuF_4$:50% Yb^{3+}/2% Er^{3+}, and $NaYbF_4$:2% Er^{3+}, which were taken with consistent exposure time of 0.1, 0.02, and 1 s, respectively, directly indicating the dependence of the overall emission color on the concentration of the Yb^{3+} ion.

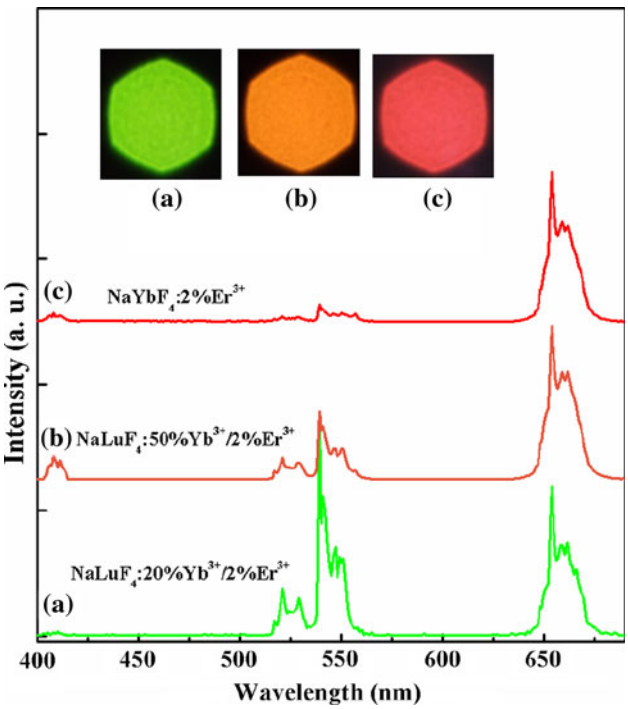

Fig. 5 Upconversion spectra of the $NaLuF_4$:20% Yb^{3+}/2% Er^{3+} (*a*), $NaLuF_4$:50% Yb^{3+}/2% Er^{3+} (*b*), and $NaYbF_4$:2% Er^{3+} (*c*) samples under 980 nm LD excitation (normalized to Er^{3+} green emission). *Inset* shows the corresponding digital photograph taken with exposure time of 0.1, 0.02, 1 s, respectively

Upconversion mechanisms

The emission spectra of Er^{3+} or Tm^{3+} in $NaLuF_4$ host have been measured and analyzed based on the variation of the concentration of emitters Er^{3+} and Tm^{3+} and sensitizer Yb^{3+}. Combing green and red emissions of $NaLuF_4$:Yb^{3+}/Er^{3+} with blue emission of $NaLuF_4$:Yb^{3+}/Tm^{3+}, three primary colors were produced in this high efficient $NaLuF_4$ host under the infrared excitation. Whether the emission mechanism in the $NaLuF_4$ microtubes is different from the ever reported results? In order to investigate deeply the involved upconversion mechanisms in the $NaLuF_4$:Yb^{3+}/Er^{3+} and the $NaLuF_4$:Yb^{3+}/Tm^{3+} microtubes, the intensities of the upconversion emission were recorded by integrating the emission spectra, of which the dependences on the 980 nm LD pump power were presented in the log–log plot (Fig. 6). It is well known that the visible emission intensity (I_{em}) is proportional to a certain power (n) of the infrared (IR) excitation intensity (I_p): $I_{em} \propto I_p^n$, where n is the number of IR photons absorbed per visible phonon emitted. As seen from Fig. 6a, the $^1D_2 \rightarrow {}^3F_4$ and $^1G_4 \rightarrow {}^3H_6$ upconversion emission intensities of Tm^{3+}demonstrated cube power dependencies and the $^1G_4 \rightarrow {}^3F_4$ emission intensity exhibited quadratic power dependencies, indicating three and two photon upconversion mechanisms, respectively. Based on the simplified energy level diagram and sequential photon absorption and energy transfer steps [17, 29, 35] in Fig. 7, under the excitation of 980 nm LD, the Yb^{3+} ion in ground state ($^2F_{7/2}$) absorbs a 980 nm photon and populates the $^2F_{5/2}$ level. Energy transfer from an Yb^{3+} ion in the $^2F_{5/2}$ state to an adjacent ground Tm^{3+} ion populates the $^3H_5$ level. The Tm^{3+} ion in the $^3H_5$ level can then relax nonradiatively (without emission of photons) to the $^3F_4$ level. Similarly, after three subsequent excitation energy transfers from Yb^{3+} ions, the Tm^{3+} is promoted to the $^1D_2$ and $^1G_4$ levels, and then dropped back to the low-energy $^3F_4$ and $^3H_6$ levels, which leads to the blue $^1D_2 \rightarrow {}^3F_4$, $^1G_4 \rightarrow {}^3H_6$, and the red $^1G_4 \rightarrow {}^3F_4$ emissions. However, it is noted that the ground state of

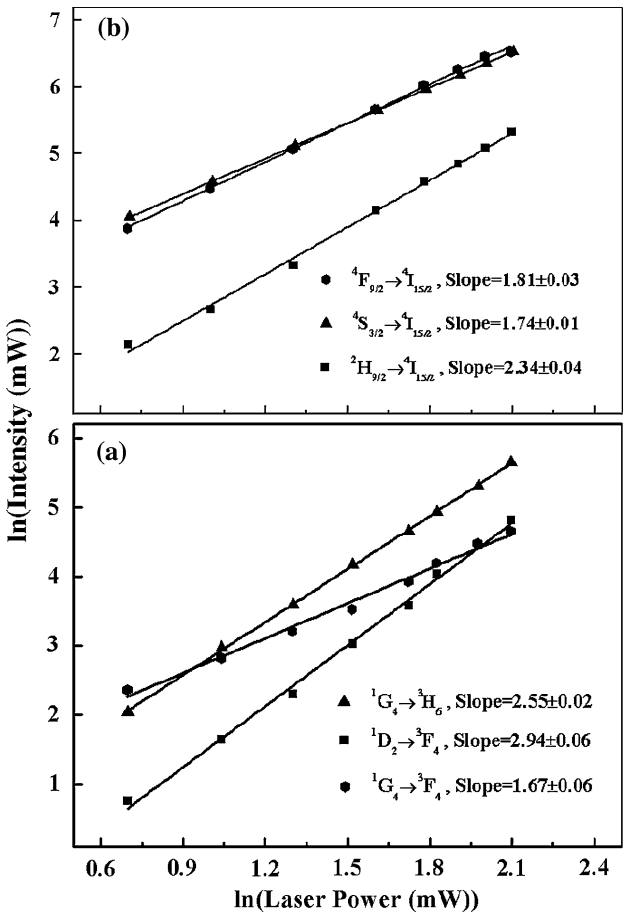

Fig. 6 Power dependence of the upconversion emissions for the $NaLuF_4$:20% Yb^{3+}/0.8% Tm^{3+} (**a**) and $NaLuF_4$:20% Yb^{3+}/2% Er^{3+} (**b**) microtubes under 980 nm LD excitation

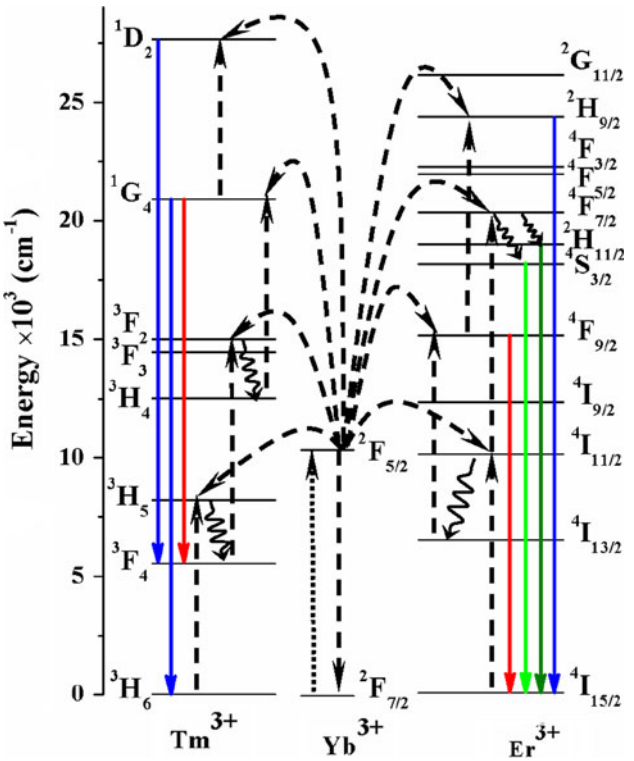

Fig. 7 Schematic of the upconversion luminescence processes in the Yb^{3+}/Tm^{3+}, Yb^{3+}/Er^{3+}-codoped $NaLuF_4$ under 980 nm LD excitation. The *full*, *dotted*, *dashed*, and *curly arrows* represent emission, photon excitation, energy transfer, and multiphoton relaxation, respectively

Tm^{3+} needs to absorb four pumping photons for population of $^1D_2$ level, which seems conflicting with the above addressed three photon process for the $^1D_2 \rightarrow {}^3F_4$ transition. Considering this confliction, it can be inferred based on the saturation effect that some energy levels have taken a nearly saturated population in the upconversion processes for populating the $^1D_2$ level of Tm^{3+} ion. Based on the proposed upconversion mechanism, the $^3F_4$ level is addressed to take a nearly saturated population which results the observed three photon process for $^1D_2 \rightarrow {}^3F_4$ transition. Moreover, it should be noted that the population of $^3F_4$ state is mainly attributed to the contribution of depopulation of $^3H_5$ state which is predominantly depending on the efficient energy transfer processes from Yb^{3+} to Tm^{3+} and between Tm^{3+} pairs.

For the Er^{3+} emission in $NaLuF_4$:Yb^{3+}/Er^{3+}, two photon power dependency was observed for the red emission $\left({}^4F_{9/2} \rightarrow {}^4I_{15/2}\right)$ and green emission $\left({}^4S_{3/2} \rightarrow {}^4I_{15/2}\right)$, while three photon power dependency was observed for the violet emission $\left({}^2H_{9/2} \rightarrow {}^4I_{15/2}\right)$ and shown in Fig. 6b. The excitation and emission processes can be simply described as follows:

First, an Yb^{3+} ion in the $^2F_{5/2}$ state transfer its energy to an Er^{3+} ion to populate the $^4I_{11/2}$ level. Second, energy transfer from an Yb^{3+} ion can then populate the $^4F_{7/2}$ level of the Er^{3+} ion. The Er^{3+} ion can then decay nonradiatively to the $^2H_{11/2}$ and $^4S_{3/2}$ levels lead to the occurring of transitions $^2H_{11/2} \rightarrow {}^4I_{15/2}$ and $^4S_{3/2} \rightarrow {}^4I_{15/2}$. Alternatively, the Er^{3+} ion in the $^4I_{11/2}$ level can also populate the $^4I_{13/2}$ state via the nonradiative $^4I_{11/2} \rightarrow {}^4I_{13/2}$ relaxation. The Er^{3+} ion from the $^4I_{13/2}$ level can further populate the $^4F_{9/2}$ level by absorption of a 980 nm photon, or energy transfer from an Yb^{3+} ion, which leads to the red $^4F_{9/2} \rightarrow {}^4I_{15/2}$ emission. In addition, the Er^{3+} ion in the $^4F_{9/2}$ level can be promoted to the $^2H_{9/2}$ level and so weak blue $^2H_{9/2} \rightarrow {}^4I_{15/2}$ emission occurs.

It is worth noting that the slope value of the $^2H_{9/2} \rightarrow {}^4I_{15/2}$ is equal to 2.34 that is remarkably lower than the theoretical value of 3. For this slope deviation between theory and experiment, similar with the above demonstration for $^1D_2 \rightarrow {}^3F_4$ transition, it was ascribed to the saturation effect of $^4I_{11/2}$ level which leads to the low-slope value (2.34) of $^2H_{9/2} \rightarrow {}^4I_{15/2}$ transition. The saturation of

the $^4I_{11/2}$ level has been observed in some previously reported study [36], which can be addressed to the efficient energy transfer from the $^2F_{5/2}$ level of Yb^{3+} to the $^4I_{11/2}$ level of Er^{3+} and resonant energy transfer between the $^4I_{11/2}$ level pairs and between $^4I_{15/2} \rightarrow {}^4I_{11/2}$ and $^4F_{7/2} \rightarrow {}^4I_{11/2}$ transitions.

Conclusion

In conclusion, Re-doped $NaLuF_4$ microtubes with uniform size were synthesized via a facile hydrothermal approach. The XRD results confirmed the purity of the β-$NaLuF_4$ phase of these microtubes of 3 μm in diameter and 40 μm in length. Under 980 nm LD excitation the as-obtained $NaLuF_4$:20% Yb^{3+}/0.8% Tm^{3+}, $NaLuF_4$:20% Yb^{3+}/2% Er^{3+}, $NaLuF_4$:50% Yb^{3+}/2% Er^{3+}, and $NaYbF_4$:2% Er^{3+} microtubes exhibit intense upconversion blue, green, yellow, and red light, respectively. The involved upconversion mechanisms were discussed in these Re-doped $NaLuF_4$ microtubes based on emission spectra, the plot of luminescence intensity to pump power and a simplified energy level diagram. These synthesized lanthanide-doped β-$NaLuF_4$ microtubes might be an idea candidate for substituting conventional phosphors in comparison to the reported non-hollow $NaReF_4$ materials.

Acknowledgements Authors are grateful for the support from Scientific Research Fund of Hunan Provincial Education Department under Grant no. 07C283 and critical reading by C. Q. Sun at Nanyang Technological University, Singapore.

References

1. Schafer H, Ptacek P, Kompe K, Haase M (2007) Chem Mater 19:1396
2. Shalav A, Richards BS, Trupke T, Kramer KW, Gudel HU (2005) Appl Phys Lett 86:013505
3. Downing E, Hesselink L, Ralston J, Macfarlane R (1996) Science 273:1185
4. Qiu J, Miura K, Inouye H, Kondo Y, Mitsuyu T, Hirao K (1998) Appl Phys Lett 73:1763
5. Chatterjee DK, Rufaihah AJ, Zhang Y (2008) Biomaterials 29:937
6. Hilderbrand SA, Shao F, Salthouse C, Mahmood U, Weissleder R (2009) Chem Commun 28:4188
7. Laroche M, Girard S, Moncorgé R, Bettinelli M, Abdulsabirov R, Semashko V (2003) Opt Mater 22:147
8. Heng-fu P, Pu W, Xiao-feng F, Rui-hua W, Bao-sheng L (1996) Chinese Phys Lett 13:602
9. Yoshida H, Ikuhara Y, Sakuma T (2001) J Mater Res 16:716
10. Chen D, Yu Y, Wang Y, Huang P, Weng F (2009) J Phys Chem C 113:6406
11. Mai H-X, Zhang Y-W, Si R, Yan Z-G, Sun L-d, You L-P, Yan C-H (2006) J Am Chem Soc 128:6426
12. Jia G, You H, Song Y, Jia J, Zheng Y, Zhang L, Liu K, Zhang H (2009) Inorg Chem 48:10193
13. Li C, Yang J, Yang P, Zhang X, Lian H, Lin J (2008) Cryst Growth Des 8:923
14. Zhuang JL, Liang LF, Sung HHY, Yang XF, Wu MM, Williams ID, Feng SH, Su Q (2007) Inorg Chem 46:5404
15. Li C, Yang J, Quan Z, Yang P, Kong D, Lin J (2007) Chem Mater 19:4933
16. Li C, Quan Z, Yang J, Yang P, Lin J (2007) Inorg Chem 46:6329
17. Boyer J-C, Vetrone F, Cuccia LA, Capobianco JA (2006) J Am Chem Soc 128:7444
18. Naccache R, Vetrone F, Mahalingam V, Cuccia LA, Capobianco JA (2009) Chem Mater 21:717
19. Wang X, Zhuang J, Peng Q, Li Y (2005) Nature 437:121
20. Zhang F, Zhao D (2008) ACS Nano 3:159
21. Liang L, Xu H, Su Q, Konishi H, Jiang Y, Wu M, Wang Y, Xia D (2004) Inorg Chem 43:1594
22. Fang YP, Xu AW, You LP, Song RQ, Yu J, Zhang HX, Li Q, Liu HQ (2003) Adv Funct Mater 13:955
23. Jia G, Liu K, Zheng Y, Song Y, Yang M, You H (2009) J Phys Chem C 113:6050
24. Sun CQ, Li S, Tay BK, Chen TP (2002) Acta Mater 50:4687
25. Pan LK, Sun CQ, Tay BK, Chen TP, Li S (2002) J Phys Chem B 106:11725
26. Suyver JF, Grimm J, van Veen MK, Biner D, Kramer KW, Gudel HU (2006) J Lumin 117:1
27. Chen G, Ohulchanskyy TY, Kumar R, Ågren H, Prasad PN (2010) ACS Nano 4:3163
28. Boyer J-C, Cuccia LA, Capobianco JA (2007) Nano Lett 7:847
29. Wang F, Liu X (2009) Chem Soc Rev 38:976
30. Wang F, Liu X (2008) J Am Chem Soc 130:5642
31. Wang G, Peng Q, Li Y (2009) J Am Chem Soc 131:14200
32. Mai H-X, Zhang Y-W, Sun L-D, Yan C-H, Phys J (2007) Chem C 111:13721
33. Li Z, Zhang Y (2008) Nanotechnology 19:345606
34. Vetrone F, Boyer J-C, Capobianco JA, Speghini A, Bettinelli M (2004) J Appl Phys 96:661
35. Wang L, Li Y (2007) Chem Mater 19:727
36. Chen G, Somesfalean G, Liu Y, Zhang Z, Sun Q, Wang F (2007) Phys Rev B 75:195204